The influence of grain rotation on the structure of dust aggregates

Paszun D [a], Dominik C. [a]

[a] *Astronomical Institute "Anton Pannekoek", University of Amsterdam, Kruislaan 403 1098 SJ Amsterdam, The Netherlands*

Abstract

We study the effect of rotation during the collision between dust aggregates, in order to address a mismatch between previous model calculations of Brownian motion driven aggregation and experiments. We show that rotation during the collision does influence the shape and internal structure of the aggregates formed. The effect is limited in the ballistic regime when aggregates can be considered to move on straight lines during a collision. However, if the stopping length of an aggregate becomes smaller than its physical size, extremely elongated aggregates can be produced. We show that this effect may have played a role in the inner regions of the solar nebula where densities were high.

Key words: Origin, Solar System, Interplanetary Dust

1 Introduction

Dust aggregation plays a central role in most theories of planet formation. While for the formation of giant planets, disk instability scenarios continue to be discussed (Boss, 1997), dust aggregation certainly stands at the beginning of the formation of planetesimals and therefore of the terrestrial planets. Independent of the detailed process that finally forms planetesimals (e.g. Weidenschilling, 1980; Youdin and Shu, 2002; Cuzzi et al., 2001), dust grains first need to grow and settle towards the midplane of the disk. Planet formation therefore starts with the first steps of dust aggregation, when dust grains inherited by the disk from the interstellar medium start to collide and grow. This first step of growth is governed by Brownian motion aggregation. In the high density regions of the disk, dust/gas coupling is so tight that the main source of relative velocities between grains are the random motions produced by individual collisions between gas atoms and the grains. Understanding the

Brownian motion phase of dust aggregation therefore means understanding the first step towards planets in disks.

At the very low collision velocities produced by Brownian motion ($\sim$cm/s), grains always stick and no restructuring is occurring in the collision (Dominik and Tielens, 1997; Blum and Wurm, 2000). The structure of aggregates formed in this regime is therefore indeed a pure probe of the physical processes driving growth with Brownian motion of the particles. Theoretically, growth by Brownian motion was studied for example by Kempf et al. (1999). They calculated the motion of micron sized dust grains enclosed in a box of approximately constant dust number density. Diffusion, caused by the presence of a gaseous medium, produces relative motion of grains and leads to the growth of dust. The orientation of the (spherically not symmetric) aggregates was not followed during the computations. Instead, in order to randomize the relative orientation during collisions, the orientations of collision partners just before a collision was selected randomly. With these initial conditions, the aggregates were left to collide, without considering rotation *during* the collision. The calculations show a slow growth of the dust aggregates with time. At any time, the box contains a distribution of aggregate shapes which is characterized by a distribution of fractal dimensions. The mean fractal dimension found in the numerical study is around $D_f = 1.8$.

On the experimental side, a series of low-gravity experiments has been conducted (Blum et al., 2000; Krause and Blum, 2004) in order to study the growth of fractal aggregates under Brownian motion conditions. The results confirm many expected aspects of this growth regime, but also showed unexpectedly elongated aggregates, in contrast with the predictions by Kempf et al. (1999).

The authors qualitatively argue that rotation of the aggregates during the collision might lead to more elongated aggregates, because the probability of achieving contact between two aggregates at larger separations increases if the aggregates rotate.

To compare experimental and theoretical results, it is necessary to quantify the visual impression of *elongation*. In this study we will be using two different ways to do so:

(1) One can define an **elongation factor** as the ratio of maximum to minimum diameter of aggregate

$$f_{\mathrm{el}} = \frac{d_{\mathrm{max}}}{d_{\mathrm{min}}} \tag{1}$$

where d_{min} is measured in perpendicular direction to d_{max}. Experimentally, this quantity has to be derived from a few, or even a single picture.

When measuring this value for model aggregates, we therefore choose three different projections of the aggregate and determine $d_{\max}$ and $d_{\min}$ from these images.

(2) We can also derive the **fractal dimension** of the aggregates. This quantity can be computed by measuring the mass–radius relation of aggregates of different mass m and size R. If that relation follows a power law

$$m \propto R^{D_{\mathrm{f}}} \tag{2}$$

then D_{f} is called the fractal dimension of the aggregate. The fractal dimension measured in the experiments is 1.4, and typical values predicted by the numerical calculations are around 1.8, indicating a mismatch.

While the idea of particle rotation is appealing as a mechanism to increase the elongation of dust aggregates, this has never been shown quantitatively. In this paper we investigate the influence of rotation on the structure of aggregates formed under Brownian motion conditions.

2   The model

In order to test the influence of rotation on the growth of aggregates we developed a model for collisions of rotating aggregates. Since we are interested in the low velocity regime, collisions are not energetic enough to cause restructuring. These processes are therefore neglected, and aggregates are treated as rigid entities. Our code calculates the equation of motion of two aggregates set on collision course with each other. When both aggregates get into the first contact between any two constituent grains, a new aggregate is formed. The structure of this aggregate is determined by the position and orientation of the two aggregates at the moment of contact – no further changes occur after this moment.

In all our calculations we used the same monomers sizes and masses as in the CODAG experiment (Krause and Blum, 2004). Each monomer was 1μm in diameter and its mass was 1.0×10^{-15} kg. The temperature assumed in our calculations was 300K , again like in the experiment.

In a fully general calculation, one would have to consider an ensemble of particles and follow the growth of this ensemble. However, it has been shown experimentally that the mass distribution function during Brownian motion growth is very narrow, so that a mono-disperse approximation works very well (Krause and Blum, 2004). We therefore proceeded in the following way: Starting with dimers, we first compute a large number of collisions between dimers, with random initial position, rotational orientation, and impact parameter.

The translational and rotational velocities are taken from a Maxwellian distribution for a given temperature T. The resulting quadrumer structures are stored in a database. In the next step, we collide two quadrumers selected randomly from the database. A database of quadrumer structures is built in this way. In a similar way, we produce aggregates with larger sizes, always containing 2^n grains.
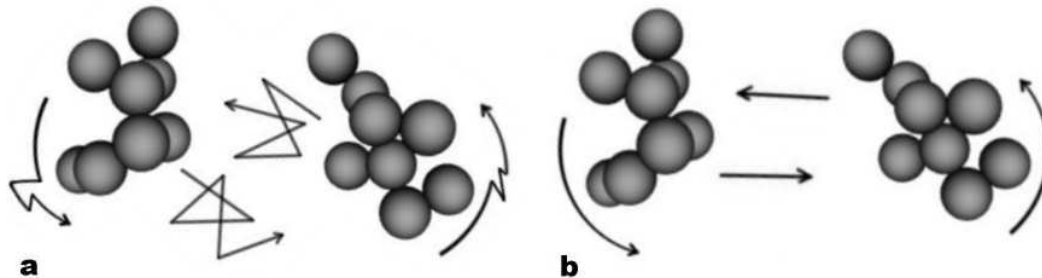

Fig. 1. Schematic sketch of collisions between two aggregates in two cases. a - non–ballistic collision with mean free path of an aggregate shorter than the aggregate size. Velocities change every τ_{f}. b - ballistic collisions with mean free path longer than size of an aggregate.

In order to solve the problem we have studied the influence of rotation in two separate cases. The first one assumes *ballistic collisions* where the mean free path of an aggregate is longer than its size. The second assumes aggregation in a *non–ballistic regime*. The stopping length in this case is shorter than the size of the aggregate.

2.1 Ballistic collisions

In the ballistic regime, the mean free path of all involved particles is larger than the size of the largest particle. In this case, the center of mass of each particle moves on a straight line during the collision. In physical terms, the ballistic limit is reached in the limit of low (but non–zero, because the gas still needs to cause Brownian motion of the grains) gas densities. This is generally assumed to be the case both in protoplanetary disks, and in microgravity experiments described above.

When aggregates are colliding without rotation and on linear trajectories, elongated aggregates are formed when the first contact is made between grains on the outside of the aggregate, while the two aggregates are more or less aligned. Depending on the initial orientation, this situation is realized for different impact parameters: If the aggregates are aligned along the direction of relative motion between the colliding aggregates, a small impact parameter is needed. If the alignment is perpendicular to the collision direction, a large impact parameter produces the most elongated result, while a small impact

parameter would lead to a more compact structure. If the aggregates are rotating during approach, the chances that the contact will be made early with an elongated geometry increase. For this process to be efficient, the linear speed of grains far away from the center of mass should be comparable or larger than the translational motion. Therefore, the larger the ratio of rotational and translational speeds are, the greater the average elongation of the aggregate becomes.

This can be achieved in two ways. Superthermal grain rotation does occur in interstellar space, where it is responsible for the alignment of non–spherical grains with the galactic magnetic field and in this way produces the interstellar polarization (Purcell, 1979). With superthermal rotation, a fast circular motion is induced while the linear velocity remains thermal. However, superthermal rotation relies on small forces like non–isotropic absorption and scattering of light (Draine and Weingartner, 1996), or H_2 formation on specific sites (Purcell, 1979), to accelerate the grains. The non–thermal rotation speeds can only be sustained at extremely low gas densities. In fact, the densities prevailing in protoplanetary disks are prohibitive, and superthermal rotation can be ruled out there (Ossenkopf, 1993).

On the other hand, the effective linear translational speed can be slowed down by embedding the grains into gas of high density, leading into the regime of non–ballistic collisions.

2.2   Non–ballistic collisions

The mean free path $l_{\mathrm{b}} = v_{\mathrm{th}}\tau_{\mathrm{f}}$ of a dust grain is the distance an aggregate with mean thermal velocity v_{th} can move during one friction time. The friction time of a dust grain is

$$\tau_{\mathrm{f}} = \varepsilon \frac{m}{\sigma_{\mathrm{a}}} \frac{1}{\rho_{\mathrm{g}} v_{\mathrm{m}}} \tag{3}$$

where m, σ_{a}, ρ_{g} and v_{m} are mass, aerodynamical cross section, gas density and mean thermal velocity of the gas molecule respectively and ε is a proportionality coefficient which is around 0.6 (Blum et al., 1996).

If ρ_{g} increases, the mean free path decreases accordingly. When the mean free path becomes similar to the largest aggregate involved in the collision, the assumption of a ballistic collision is no longer valid. Instead, the particle execute a random walk both in linear motion and in rotation. On average, the aggregates will spent a longer time at large distances before moving closer together. This effect increases the chance of creating a contact already at large

5

distances, i.e. a strongly elongated aggregate. Fig. 1a presents the schematic picture of a non–ballistic collision.

3   Results

In order to investigate the influence of rotation on the production of elongated aggregates, we calculated growth of rotating aggregates in the range from ballistic to highly non—ballistic collisions.

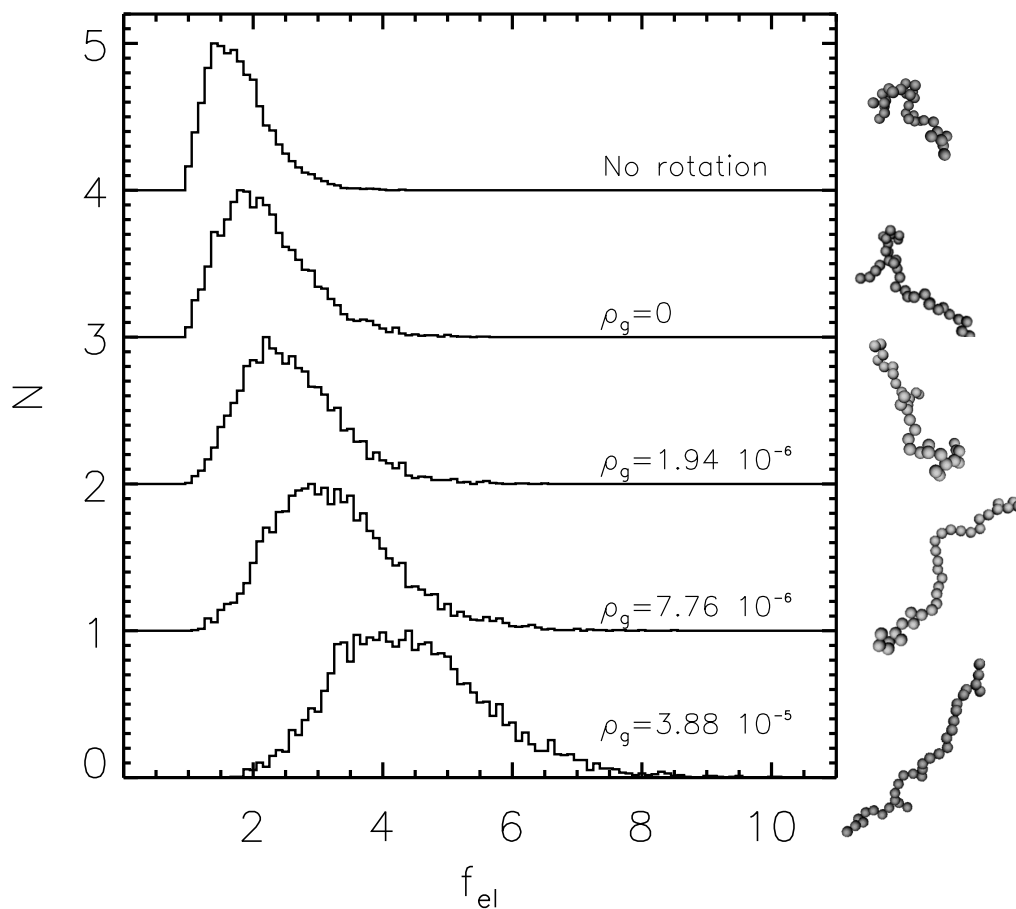### 3.1   Ballistic collisions with and without thermal rotation

Fig. 2.   Distribution of elongation factors, with peak value normalized to unity. From top to bottom: non–rotation case, ballistic thermal rotation, thermal rotation for different gas densities ρ_g in $g\,cm^{-3}$. The distributions are shifted vertically for better visibility.

Distributions of f_{el} for ballistic collisions are plotted in fig. 2. In order to be able to compare with the results of Kempf et al. (1999), we also computed a

case with rotation turned of. The two top diagrams show the non–rotating case and thermal rotation case in the ballistic regime. For the non–rotating case, a very narrow distribution results. This distribution peaks at a value $f_{el} \approx 1.6$. For thermal rotation, the peak value shifts to $f_{el} \approx 2$ and the distribution becomes wider. For both cases, a very small fraction of particles with elongation factors 4 and larger are produced, due to fortuitous initial conditions in the computation. Fig. 3 shows the mean elongation factors as a function of aggregates size. Each point is plotted together with its $\pm 1\sigma$ errorbars. The no rotation case clearly has the lowest elongations and, as in the thermal rotation case, the line is almost flat for bigger sizes, meaning the growth affects the elongation very weakly. The elongation factors for rotating aggregates are shifted upwards from values of about $f_{el} = 1.8$ to about $f_{el} = 2.3$. The effect of rotation is also clearly seen in the fractal dimensions (fig. 4) which reach level of $D_f \approx 1.7$ for non–rotating collisions. Thermal rotation causes the fractal dimension to drop to a value of 1.46.

3.2 Rotating aggregates outside of the ballistic limit

Further calculations were done for higher gas densities. In this case, the friction length l_b becomes comparable to or shorter than the size of the colliding aggregates. While the thermal velocity decreases with increasing size (mass) of an aggregate, $\tau_f \approx$ const for small, non–compact aggregates. Consequently, the mean free path $l_b = \tau_f v_{th}$ decreases with increasing particle size. We performed calculations for several different gas densities. By tuning the gas density, we can study the transition from the ballistic to the non–ballistic regime. Fig.2 shows the resulting distribution of elongation factors for different gas densities. Fig. 3 presents the relation between the mean elongation factor and the aggregate size for different gas densities.

The mean elongation factor f_{el} depends strongly on the gas density ρ_g in the transition regime. Increasing the gas density from 10^{-6} to a few times $10^{-5} \mathrm{g\,cm^{-3}}$ strongly broadens the elongation factor distribution and shifts the peak value to $f_{el} \approx 4$. Extreme values of up to $f_{el} = 10$ are reached in the tail of the distribution function. The elongation factor also depends on size of aggregates: Larger aggregates reach the largest elongations. This is the result of the decrease of the mean free path with increasing aggregate size. The elongation - size relation becomes steeper for higher gas densities. The mean elongation factor in our calculations follows a power law dependence on the gas density. The power index is size dependent. Aggregates consisting of 32 monomers follow a power law with index of 0.18, while the index for those made of 16 monomers is 0.13. This means that the latter aggregates can reach a mean elongation factor value about 3.4 for gas density $\rho_g = 3.88 \times 10^{-5} \mathrm{g\,cm^{-3}}$. For this gas density and aggregates bigger than 32 monomers the mean elongation
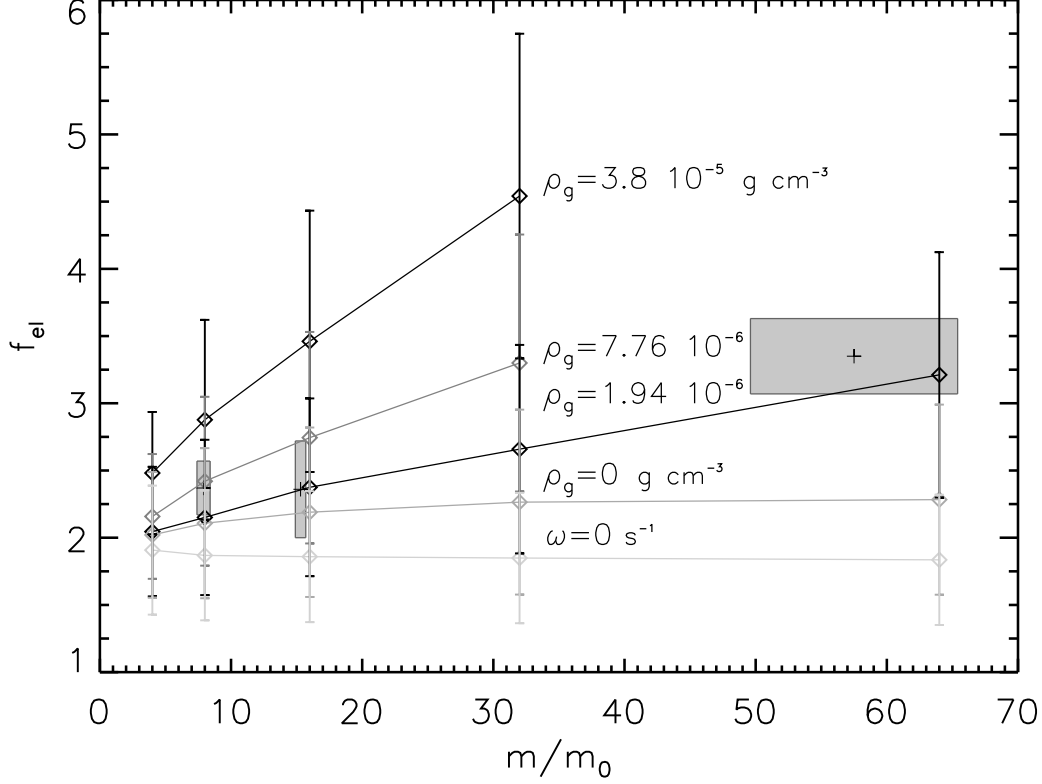
Fig. 3. Mean elongation factor for different gas densities. $\rho_{\mathrm{g}} = 0$ indicates the limiting case for low densities (mean free path much larger than aggregate sizes). The bottom line shows the elongation factor for non–rotation case. Three boxes are measured elongation factors of agglomerates formed in the CODAG experiment with $\pm 1\sigma$ errorbars (Blum & Krause personal communication).

factor reaches values above 4.5.

Fig. 3 presents also results of the CODAG experiment (Blum & Krause, personal communication). Three points together with their $\pm 1\sigma$ errorbars show the ratio of maximum to minimum diameter of aggregates formed during the experiment. An excellent fit with our calculations seems to be $\rho_{\mathrm{g}} = 1.94 \times 10^{-6}$ g cm^{-3} or slightly higher. The density used in the experiment was $\rho_{\mathrm{g}} = 2.25 \times 10^{-6}$ g cm^{-3} (Krause and Blum, 2004).

We also calculated the fractal dimension D_{f} by fitting a power law function to the plot of mean aggregate mass versus mean radius of gyration r_{g}. The average was taken over the entire distribution of particles created for the given mass. The fractal dimension as a function of the gas density is shown in Fig.4. For large densities, D_{f} appears to follow a power law with index $\alpha = -0.062$. Thus for a gas density $\rho_{\mathrm{g}} = 3.88 \times 10^{-5}$ the fractal dimension reaches the value 1.11. At low gas densities, the fractal dimension asymptotically approaches a value of 1.46, slightly larger than $D_{\mathrm{f}} = 1.41$ as observed in the CODAG experiment. Indeed, it turns out that the CODAG experiment is operating close to, but
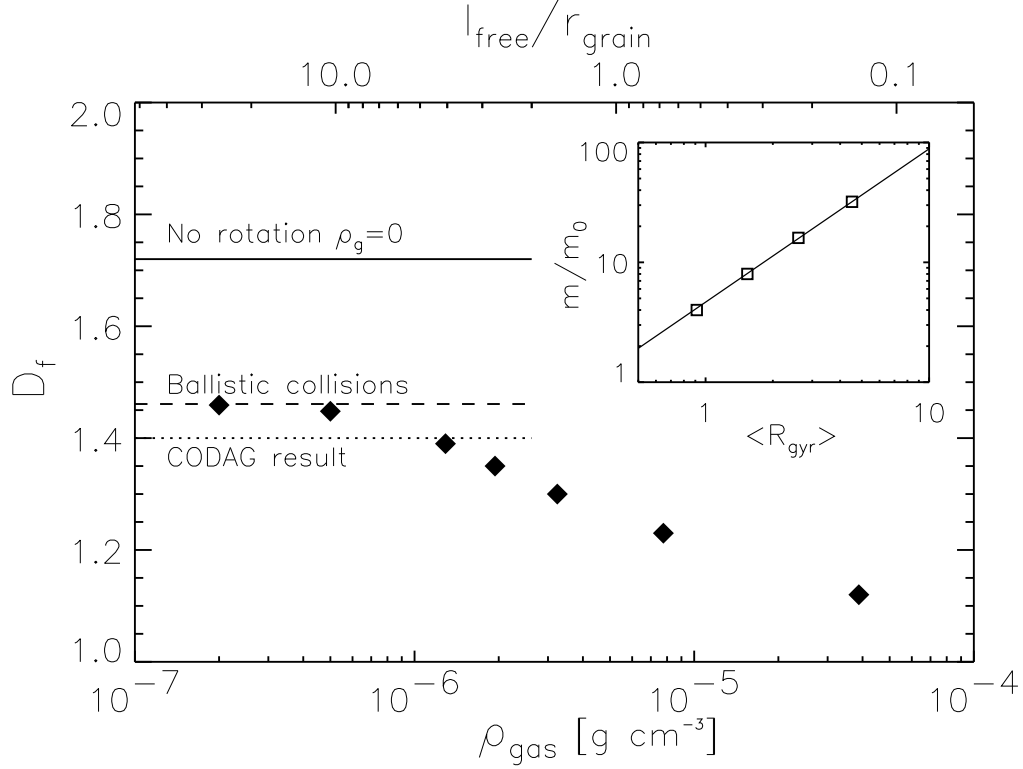
Fig. 4. Fractal dimension as a function of gas density. The upper x-axis shows the mean free path of a monomer in units of the monomer radius. The horizontal lines show the CODAG measurements ($D_f = 1.4$), the limiting result for $\lim_{\rho \to 0} D_f = 1.46$, and the result for non–rotating aggregates $D_f = 1.72$. The inset plot shows an example of fractal dimension determination by slope fitting in an r_g versus m plot, at a density of $\rho_g = 3.24 \times 10^{-6}$.

not safely within the ballistic limit. A gas density of $2.25 \times 10^{-6}\,\mathrm{g\,cm^{-3}}$ is in fact entirely consistent with $D_f = 1.4$. At this density, the mean free path of a particle is only about 1.5 grain diameters. The experiments therefore are not in the ballistic limit, but start to feel the influence of random walk during the collision. Further increasing the gas density should strongly enhance this effect, and fractal dimensions very close to unity should show up when ρ_g exceeds a few times 10^{-5} $\mathrm{g\,cm^{-3}}$.

4   Discussion

4.1   The ballistic regime

In the ballistic limit, rotation increases the collisional cross-section by producing more opportunities for a contact while two aggregates are passing each

other. In the non–rotation case only specific 'lucky' parameters (appropriate orientation and impact parameter) lead to an elongation, while rotation allows a much larger set of possible collision parameters to be effective. This effect leads to more elongated structures, because it produces significantly more opportunities for collisions with larger impact parameters.

4.2   The non-ballistic regime

In the non–ballistic regime, the random walk executed by the collision partners during a collision effectively reduces the mean (or effective) relative translational velocity. The typical distance traveled from the original position in a random walk scales with the square root of the number of steps N, we can define an effective translational speed by

$$< v > = \frac{\sqrt{N} l_{\mathrm{b}}}{N \tau_{\mathrm{f}}} \quad . \tag{4}$$

If we take $\sqrt{N} l_{\mathrm{b}} = L$ where L is size of the aggregate, then the mean effective translational velocity during random walk is inversely proportional to the gas density ρ_{g} (see eq. 5, 3).

$$< v > = \frac{l_{\mathrm{b}}^2}{L \tau_{\mathrm{f}}} \quad . \tag{5}$$

As the gas density increases, the effective velocity decreases and indeed leads to very long and slow collisions between aggregates. During that time, the aggregates also execute a random walk in rotation and in this way expose different parts toward each other. In the limit of large gas densities, this leads to contact being made always at maximum distance, and consequently to fully linear structures.

It is important to remember that we are only computing collisions of equal size aggregates, i.e. pure cluster-cluster aggregation (CCA). This simplification will tend to exaggerate the elongation at a given size. If monomers and small aggregates contribute significantly to the growth, slightly more compact aggregates are produced. In fact, if a size distribution of impactors is involved in the growth of a target, the growth physics is an intermediate case between pure CCA and particle-cluster aggregation (PCA). As an indication, we can compare the fractal dimension of 1.7 we found for non–rotating aggregates in pure CCA with the fractal dimension of ~ 1.8 found by Kempf et al. (1999) for a realistic size distribution.

4.3   Influence on aggregation timescale

Elongated aggregates, influenced by rotation and aggregation in non–ballistic regime, expose a larger surface to the gas and are easier targets for possible collisions with other dust grains. Just like for the particle mass, one can introduce a fractal dimension for the *cross-section* D_σ and write the relation between aggregate shape and cross-section as

$$\sigma \propto r_\mathrm{g}^{D_\sigma}. \tag{6}$$

Thus for limiting case of compact agglomerates $D_\sigma = 2$ while for linear grains it is 1. To see how the crosssection changes with aggregate size, one can combine both fractal dimensions D_σ and D_f:

$$\sigma \propto (m/m_0)^{\frac{D_\sigma}{D_\mathrm{f}}}. \tag{7}$$

The cross-section of aggregates is related to aggregation timescale by

$$t \propto \frac{1}{\sigma n v} \tag{8}$$

where t is aggregation time, n is number density of dust grains and v is velocity. We calculated cross-sections of aggregates with different fractal dimensions in order to investigate the timescale of aggregation. Fig. 5 shows the timescale divided by the timescale for the most compact aggregates. Each line corresponds to different fractal dimension D_f. The most interesting are $D_\mathrm{f} = 1.8$ which corresponds to the aggregates formed in the numerical calculations by Kempf et al. (1999) and fractal dimension $D_\mathrm{f} = 1.4$ which was obtained in the CODAG experiment (Krause and Blum, 2004). The timescale is shorter for elongated and open aggregates because of the larger cross-sections. The difference increases with increasing size of aggregates.

4.4   Application to protoplanetary disks

To assess the relevance of the effects discussed in the current paper in a protoplanetary disk, we need to compute the stopping length of dust grains as a function of aggregate size and location in the disk. The boundary condition for ballistic and non–ballistic collisions is reached when the mean free path equals the physical size of the dust aggregate approximately given by the radius of gyration: $l_\mathrm{b}(\rho_\mathrm{g}, T) = r_\mathrm{g}(m)$. This condition leads to a relation between cluster size and gas density, indicating how large the cluster should be at a
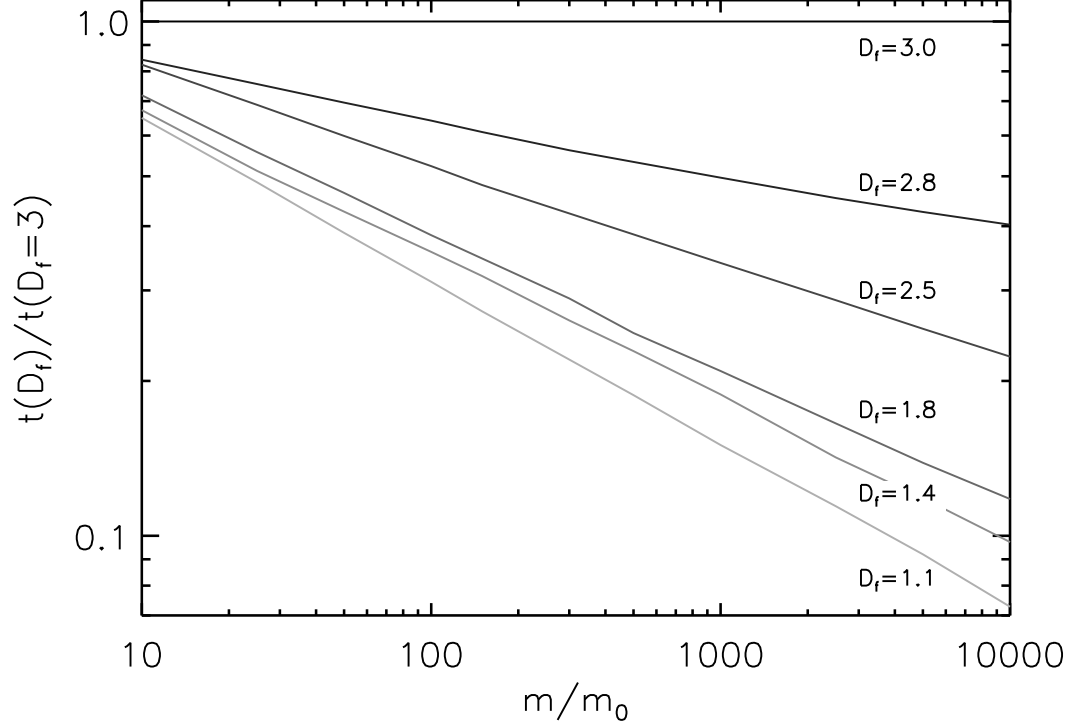
11

Fig. 5. Aggregation timescale $t \propto \frac{1}{\sigma n v}$ divided by aggregation timescale for compact agglomerates as a function of mass. Different lines correspond to different fractal dimensions. From top to bottom $D_{\mathrm{f}} = 3.0, 2.8, 2.5, 1.8, 1.4, 1.1$.

given density in order to start feeling the effect of elongation enhancement by non–ballistic collisions.

We will make the simplifying assumption that the stopping time of an aggregates is (at a given density) independent of size. This assumption is valid for very small aggregates, and for aggregates with very open structure, i.e. low fractal dimension.

We use the definition of the radius of gyration given by eq. 2 and transform it into

$$r_g(m) = B m^{\frac{1}{D_{\mathrm{f}}}} \tag{9}$$

where $B = \frac{1}{A^{1/D_{\mathrm{f}}}}$ and A is a proportionality coefficient from eq. 2. Then the relation between cluster mass and gas density relation can be derived as

$$m^{\frac{1}{D_{\mathrm{f}}} - 0.5} = \frac{\varepsilon}{B} \sqrt{\frac{3 m_{\mathrm{m}}}{8\pi}} \frac{1}{n_0 r^2 \rho_{\mathrm{g}}}, \tag{10}$$

where m_{m} is a mean mass of a gas molecule and n_0 is number of monomers in the aggregate. In order to find n_0 we substitute the cluster mass by $m = n_0 m_0$

12

where m_0 is the mass of a monomer.

$$n_0 = \left(\frac{\varepsilon}{B} \sqrt{\frac{3m_{\mathrm{m}}}{8\pi}} \frac{m_0^{0.5-\frac{1}{D_{\mathrm{f}}}}}{r^2 \rho_{\mathrm{g}}} \right)^{\frac{2D_{\mathrm{f}}}{2+D_{\mathrm{f}}}}. \tag{11}$$

Eq. 11 shows how the critical size of a cluster is dependent on the gas density. It also reveals a dependence on monomer size. We applied eq. (11) to the Hayashi model of the solar nebula (Hayashi et al., 1985). Fig. 6 shows, for the midplane
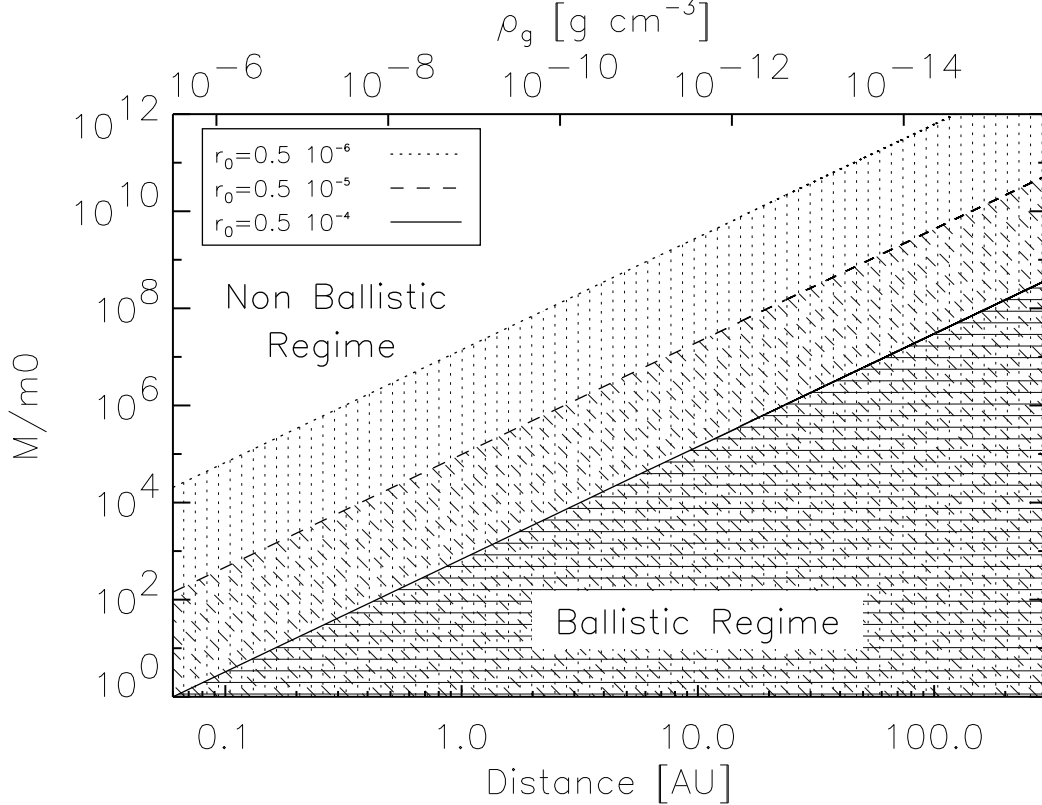

Fig. 6. Aggregate mass for which in the midplane of the solar nebula the mean free path l_{free} equals the radius of gyration r_{g}. Different lines correspond to different monomer radii r_0. The dotted line represents a monomer size of $r_0 = 0.005\,\mu m$, the dashed line $r_0 = 0.05\,\mu m$, and the solid line $r_0 = 0.5\,\mu m$. The shaded area below each line shows the ballistic regime for corresponding monomer size. The area above each line represents the non–ballistic regime. At the top of the diagram, we indicate the midplane density corresponding to the distance from the Sun, according to the Hayashi model (Hayashi et al., 1985).

density of the model, the critical size of a cluster as a function of distance from the star. Each line represents this relation for a different monomer size. Thus aggregates with a fractal dimension of $D_{\mathrm{f}} = 1.46$, are formed below the line, while above that line more elongated grains are produced. Each line is a border between the ballistic and non–ballistic regimes for a given monomer size. For

13

example, at a distance below 1 AU from the star, the gas density strongly influences the shape of aggregates formed through Brownian motion, if the aggregates consist of more than a few tens of $1\mu m$ grains. Consequently, the CODAG experiment reproduced conditions present in the inner part of the protoplanetary disk while its applicability to the low density regions in the outer disk is limited. At the CODAG density of $\rho_g = 2.25 \times 10^{-6}\,\mathrm{g\,cm^{-3}}$, the critical size is about 1.5 micron sized monomers.

5 Conclusions

We have studied the effect of aggregate rotation during collisions. The results show that rotation must definitely be treated correctly when modeling growth due to aggregation, or the geometrical structure of the resulting aggregates will be incorrect.

Rotation plays a role because it enhances the probability that two approaching aggregates make contact early on during the collision, between outer constituent grains. For the most simple case of ballistic collisions, during which the colliding aggregates move on a linear path, ignoring aggregate rotation increases the fractal dimension from 1.46 to 1.7 in the limit of pure cluster-cluster aggregation.

This effect becomes strongly enhanced if the density of the surrounding medium becomes so large that the stopping length of an aggregate becomes shorter than the aggregate size, i.e. in the non–ballistic limit. We find that reducing the stopping length to the monomer radius results in a fractal dimension of 1.25. When the stopping length is reduced to one tenth of the monomer radius, the fractal dimension drops to 1.1.

For the solar nebula, we find that non–ballistic collisions play a role in the innermost regions of the disk for even very small aggregates made of a few μm-sized grains. For smaller monomers and/or further away from the Sun, enhanced elongation can be expected for larger aggregates, made of a few 100 or 1000 grains. In the outer disk, all collisions may be considered ballistic.

14

We also thank the second (anonymous) referee for useful comments that lead to a restructuring of the manuscript.

References

Blum, J., Wurm, G., Jan. 2000. Experiments on Sticking, Restructuring, and Fragmentation of Preplanetary Dust Aggregates. Icarus 143, 138–146.

Blum, J., Wurm, G., Kempf, S., Henning, T., Dec. 1996. The Brownian Motion of Dust Particles in the Solar Nebula: an Experimental Approach to the Problem of Pre-planetary Dust Aggregation. Icarus 124, 441–451.

Blum, J., Wurm, G., Kempf, S., Poppe, T., Klahr, H., Kozasa, T., Rott, M., Henning, T., Dorschner, J., Schräpler, R., Keller, H. U., Markiewicz, W. J., Mann, I., Gustafson, B. A., Giovane, F., Neuhaus, D., Fechtig, H., Grün, E., Feuerbacher, B., Kochan, H., Ratke, L., El Goresy, A., Morfill, G., Weidenschilling, S. J., Schwehm, G., Metzler, K., Ip, W.-H., Sep. 2000. Growth and Form of Planetary Seedlings: Results from a Microgravity Aggregation Experiment. Physical Review Letters 85, 2426–2429.

Boss, A. P., 1997. Giant planet formation by gravitational instability. Science 276, 1836–1839.

Cuzzi, J. N., Hogan, R. C., Paque, J. M., Dobrovolskis, A. R., Jan. 2001. Size-selective Concentration of Chondrules and Other Small Particles in Protoplanetary Nebula Turbulence. ApJ 546, 496–508.

Dominik, C., Tielens, A. G. G. M., May 1997. The Physics of Dust Coagulation and the Structure of Dust Aggregates in Space. ApJ 480, 647–+.

Draine, B. T., Weingartner, J. C., Oct. 1996. Radiative Torques on Interstellar Grains. I. Superthermal Spin-up. ApJ 470, 551–+.

Hayashi, C., Nakazawa, K., Nakagawa, Y., 1985. Formation of the solar system. In: Protostars and Planets II. pp. 1100–1153.

Kempf, S., Pfalzner, S., Henning, T. K., Oct. 1999. N-Particle-Simulations of Dust Growth. I. Growth Driven by Brownian Motion. Icarus 141, 388–398.

Krause, M., Blum, J., Jul. 2004. Growth and Form of Planetary Seedlings: Results from a Sounding Rocket Microgravity Aggregation Experiment. Physical Review Letters 93 (2), 021103–+.

Ossenkopf, V., Dec. 1993. Dust coagulation in dense molecular clouds: The formation of fluffy aggregates. A&A 280, 617–646.

Purcell, E. M., Jul. 1979. Suprathermal rotation of interstellar grains. ApJ 231, 404–416.

Weidenschilling, S. J., Oct. 1980. Dust to planetesimals - Settling and coagulation in the solar nebula. Icarus 44, 172–189.

Youdin, A. N., Shu, F. H., Nov. 2002. Planetesimal Formation by Gravitational Instability. ApJ 580, 494–505.